Expanded View Figures

Figure EV1. PAR-3 KO does not exhibit overt defects on adherens junction formation and apical–basal polarization in the retinal vasculature.

A Staining of control and *Pard3*$^{i\Delta EC}$ P6 mice retina with adherens junction marker (VE-cadherin) and endothelial cell marker isolectin-B4 (iB4).

B Staining of control and *Pard3*$^{i\Delta EC}$ P6 retina with basement membrane marker (collagen IV), apical membrane marker (podocalyxin), and isolectin-B4 (iB4).

C Quantification of the number of sprouts/10 μm in angiogenic front. Data are presented as mean ± SEM (n = 3 retinas). Difference $^{**}P < 0.01$, analyzed by Student's t-test.

D Staining of control and *Pard3*$^{i\Delta EC}$ P6 retina artery with basement membrane marker (collagen IV), apical membrane marker (podocalyxin), adherens junction marker (VE-cadherin), and nuclei (Hoechst 33342, Sigma). 3D-reconstituted cross-section images from the region indicated with white dashed lines are shown in the images.

Data information: Scale bars: 100 μm (A and B, lower magnification), 25 μm (A and B, higher magnification), and 10 μm (D).

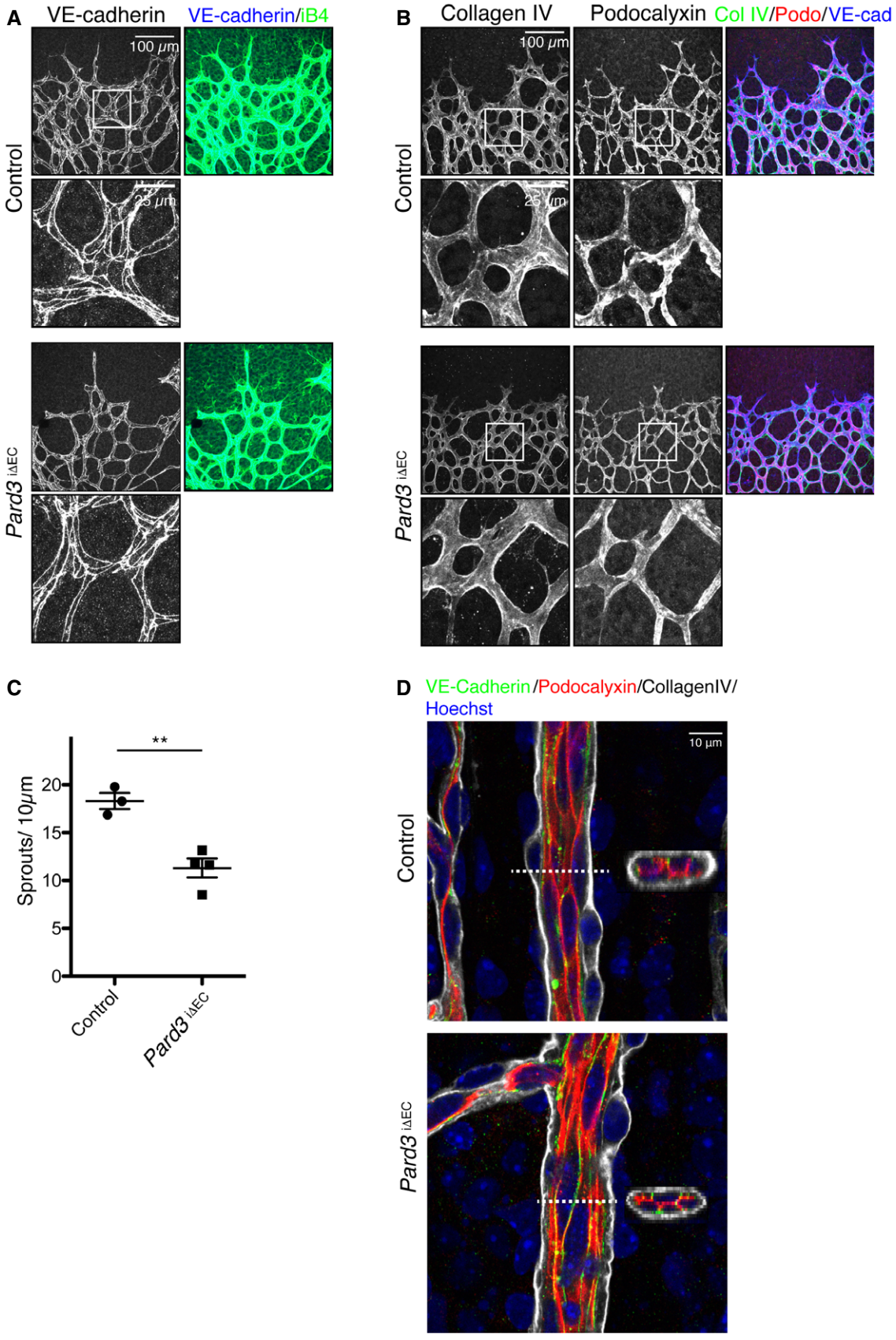
A
VE-cadherin
VE-cadherin/iB4
100 μm
25 μm
Control
Pard3 iΔEC
B
Collagen IV
Podocalyxin
Col IV/Podo/VE-cad
100 μm
25 μm
Control
Pard3 iΔEC
C
**
Sprouts/ 10μm
20
15
10
5
0
Control
Pard3 iΔEC
D
VE-Cadherin /Podocalyxin/CollagenIV/
Hoechst
10 μm
Control
Pard3 iΔEC

Figure EV1.

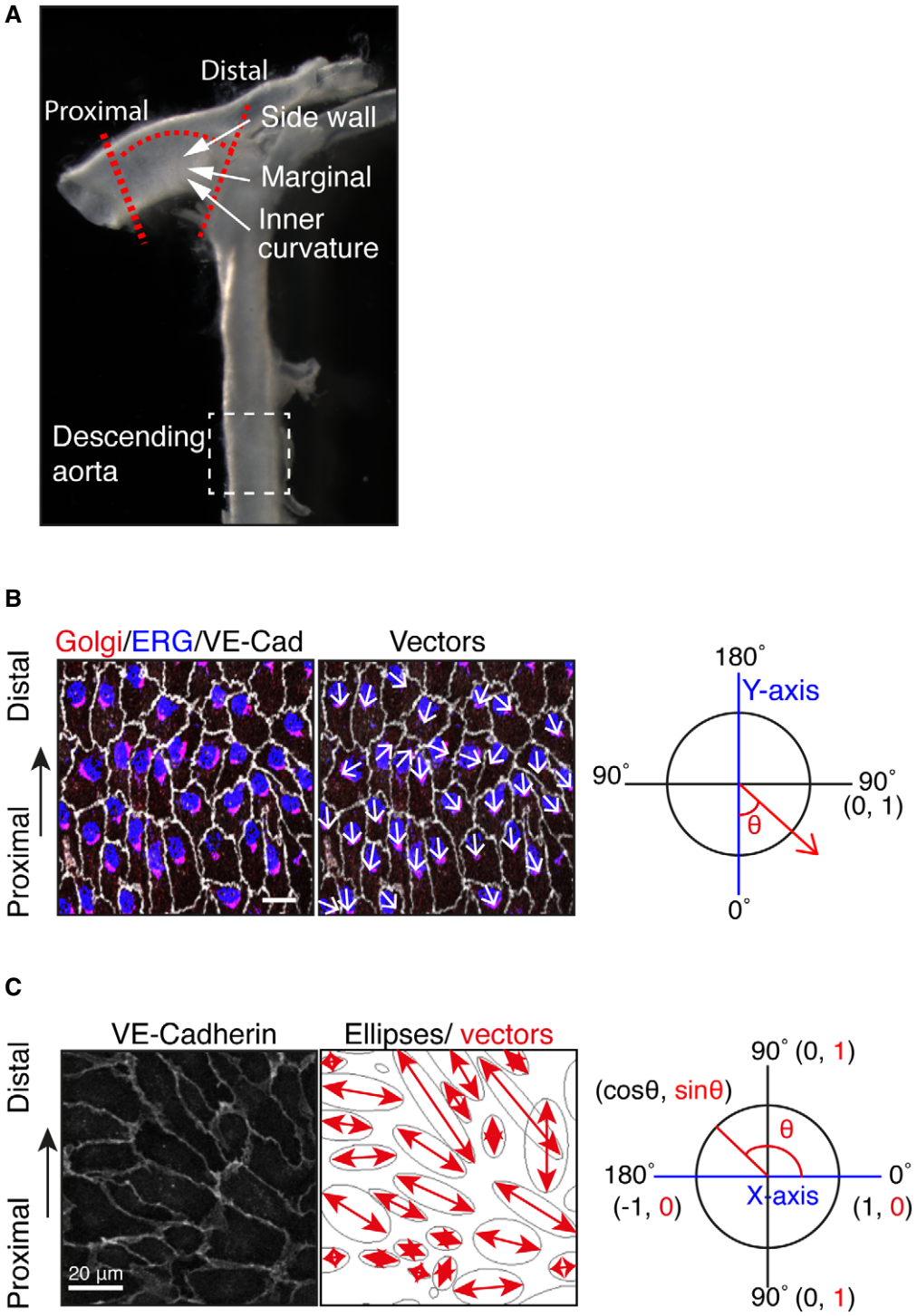

Figure EV2. Analysis of ECs in the aorta.

A To examine the effect of loss of PAR-3, the highlighted region of the aorta within the red dotted lines was dissected and analyzed.

B To quantify endothelial Golgi orientation toward flow, the angle between the axial polarity vector and the proximal–distal vector (−1 to 1) was analyzed. White arrows indicate the axial polarity vectors from each EC.

C Left panel shows the VE-cadherin signal of aorta ECs. Right panel shows the ellipse fitted to each of the EC, generated by ImageJ software. Red arrows indicate the vectors of the major axis of each ellipse. Distribution of the sin(θ) of the angle between the axial polarity vector and the proximal–distal vector was analyzed (0 to 1).

Data information: Scale bars: 20 μm (B, C).

Figure EV3. PAR-3 regulates EC Golgi reorientation toward flow *in vitro*.

A Representative images of flow chamber-cultured ECs transfected with control (Scrambled) or *PARD3*-specific siRNA (siPAR-3#1) and exposed to the indicated value of shear stress for 60 min. The cells were stained for nuclei (DAPI, blue) and Golgi apparatus (GOLPH4, red). Black arrows indicate corresponding axial polarity vectors. Flow direction is indicated on the right. Scale bar, 35 μm.

B, C Axial polarity of ECs treated with control (Scrambled) or *PARD3*-specific siRNAs (siPAR-3#1, B; or siPAR-3#2, C) in response to 12, 18, and 30 dyn/cm^2 laminar flow for the indicated time.

D Western blotting of EC lysates treated with 18 dyn/cm^2 laminar flow for indicated times, with 1 μM of 6BIO (+) or control (−) containing growth medium. Upper panels show the blot of acetylated α-tubulin (Ac α-tubulin), and lower panels show total tubulin. Quantitation of relative intensity of Ac α-tubulin is shown.

Data information: In (B and C), data are means ± SEM (n = 3 independent experiments and n = 100 cells for each experiment). In (D), data are means ± SEM (n = 3 experiments). Statistical significance (*P < 0.05; **P < 0.01) was evaluated with two-way ANOVA and Bonferroni multiple comparisons *post hoc* analysis.

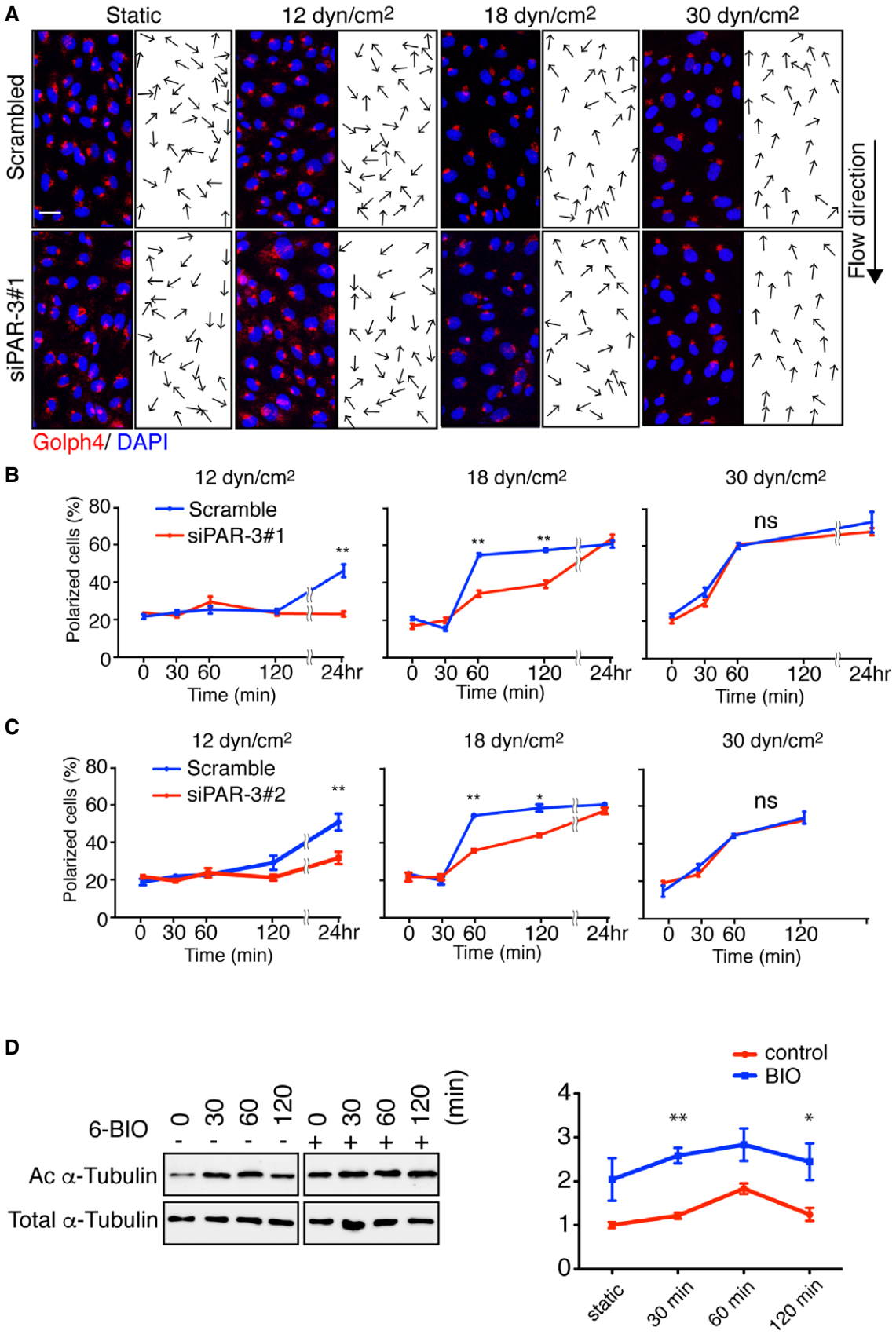

Figure EV3.

Figure EV4. Spatio-temporal antagonism of the PAR-3/aPKCλ complex versus the aPKCλ/GSK3β complex controls microtubule stabilization under flow.

A Representative time-lapse images of ECs transfected with RhoA biosensor. FRET/CFP ratio is represented in IMD mode. Cells were subjected to laminar flow of 12 dyn/cm^2 flow for 2 h. Scale bar, 15 μm.

B PLA in ECs expressing GFP-PAR-3 and myc-PKCλ in static and under 18 dyn/cm^2 flow for 1 h. Arrowheads indicate PAR-3/aPKCλ PLA signal colocalized with EC junction. Scale bar, 20 μm.

C Quantification of the images shown in (B).

D Representative images of PLA in ECs expressing GFP-GSK3β and myc-PKCλ in static (0 h) and after 1 h subjected to 18 dyn/cm^2 flow. EC junction (VE-cadherin) is green, nuclear stain (DAPI) is blue, and GFP-GSK3β is gray. Right panels show higher magnification images of the indicated areas. Yellow signals indicate PLA signal colocalized with EC junction. Scale bars, 10 μm (left panel) and 20 μm (right panel).

E Quantification of percentile of the PLA signals in the front and rear region of the ECs under static and 1-h treatment with flow.

Data information: Direction of the flow is indicated in the pictures with arrows. In (C and E), data are means ± SEM (n = 3 experiments, n = 30 cells from each experiment); statistical significance (*$P < 0.05$) was analyzed with Student's t-test (C, E).

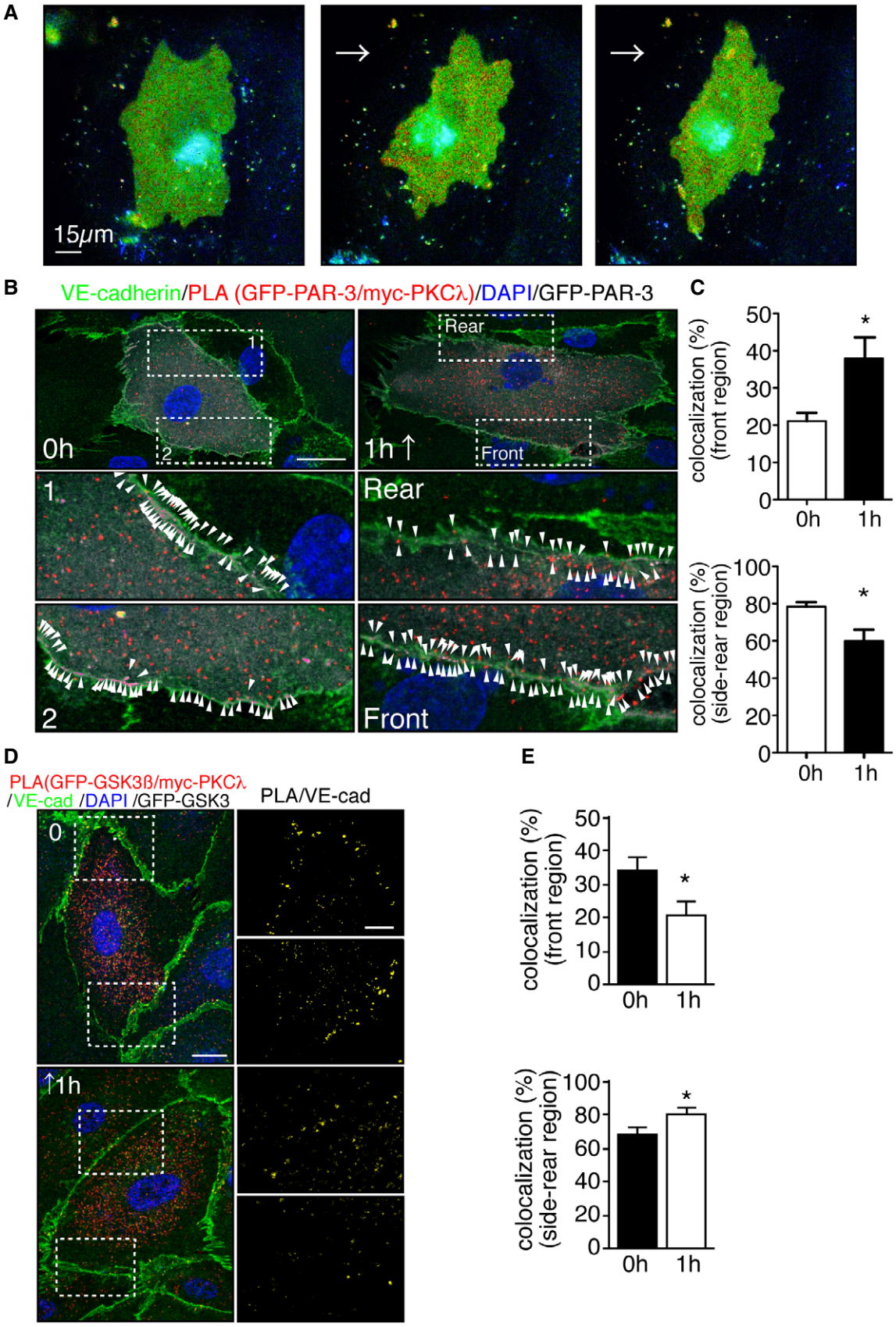

Figure EV4.

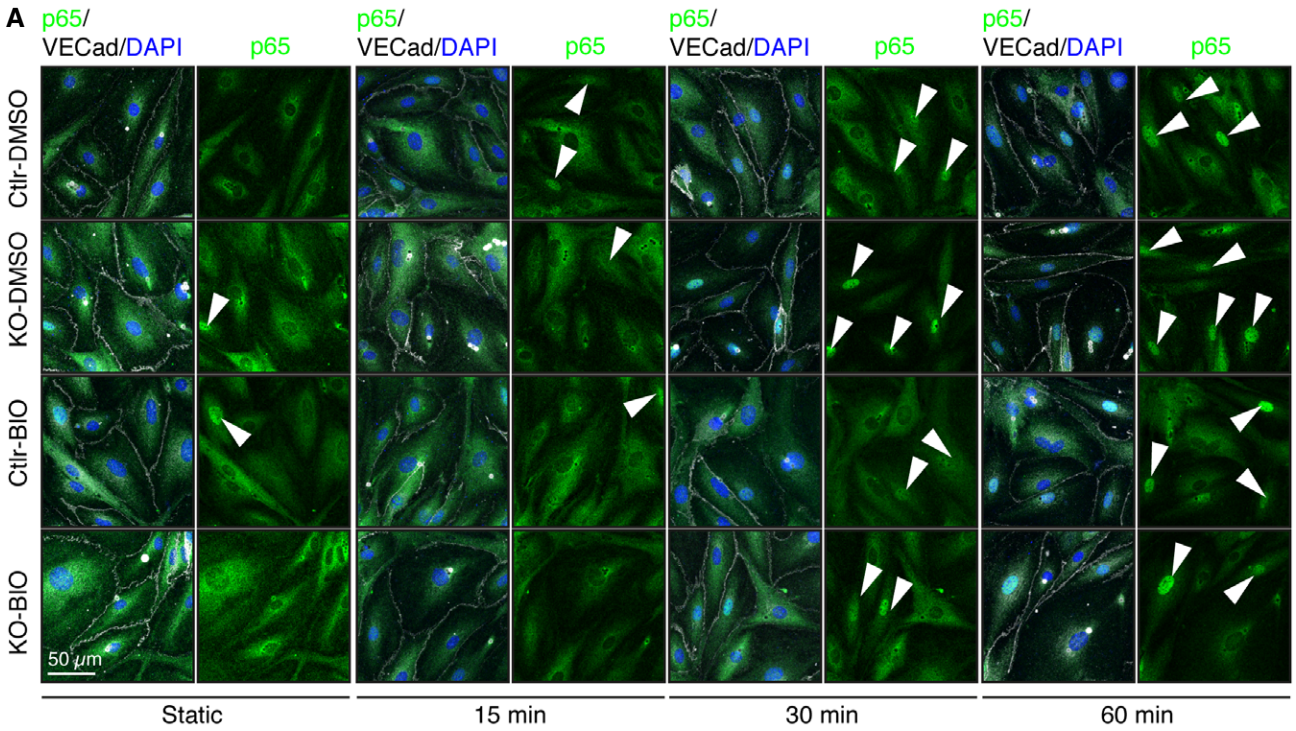

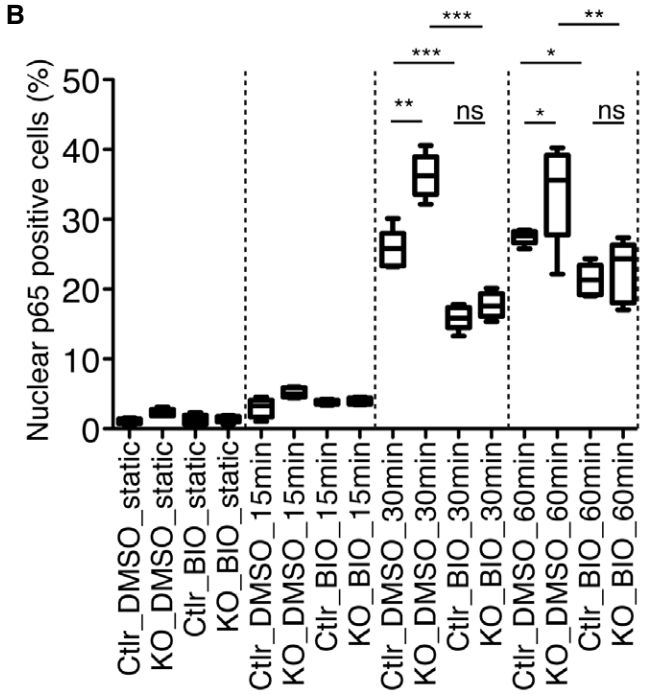

Figure EV5. PAR-3 controls nuclear localization of p65 in aortic endothelial cells in a GSK3β activity-dependent manner.

A Representative images of control and Pard3KO ECs treated with control (DMSO) or GSK3β inhibitor (6-BIO, 1 μM) under static conditions or after subjected to 12 dyn/cm^2 flow for the indicated times. EC junction (VE-cadherin) is gray, NF-κB p65 subunit (p65) is green, and nuclear stain (DAPI) is blue. Scale bar, 50 μm. White arrowheads indicate p65-positive nuclei.

B Quantitative analysis of the percentile of p65-positive ECs. Data are shown as box and whisker plots. The box spans the interquartile range, horizontal central values are median, and the whiskers extend to the highest and lowest observations (n = 50 cells); statistical significance (*P < 0.05, **P < 0.01, ***P < 0.001) was evaluated by one-way ANOVA and Tukey's multiple comparison *post hoc* analysis.